Design of Keratorefractive Surgical Procedures: Radial Keratotomy

M. R. Bryant[1]
The Aerospace Corp., M4/914,
P.O. Box 92957,
Los Angeles, CA 90009-2957

S. A. Velinsky
Associate Professor.
Department of Mechanical Engineering,
University of California—Davis,
Davis, CA 95616

By surgically incising a patient's cornea, an ophthalmologist can reduce or eliminate the patient's myopia (nearsightedness). Although one such keratorefractive procedure, known as radial keratotomy, is a common practice among some ophthalmologists, there is presently no comprehensive or universally accepted method that a surgeon can use to determine how to perform the operation to exactly eliminate a patient's refractive error. In this paper, a general methodology for designing radial keratotomy procedures that determines the optimal incision geometry on a patient-by-patient basis is presented. This approach is based on coupling a transversely isotropic finite element model of the human cornea to an optical model of the entire eye. The resulting incision geometry obtained from each design formulation not only eliminates the myopic error but yields the global minimum of the objective function.

1 Introduction

When neither glasses nor contact lenses are an acceptable means of optical correction, refractive surgery is sometimes an option. Refractive surgery refers to any surgical method of altering the refractive power of a patient's eye. In particular, keratorefractive surgeries are intended to correct refractive errors by modifying the cornea, and radial keratotomy (RK) is one of the best known and most widely used keratorefractive surgeries. As shown in Fig. 1, RK is performed by incising the eye in a radial pattern centered around the eye's aperature, or optical zone. Driven by the (intraocular) pressure of the fluid (aqueous) in the chamber behind the cornea, the deformations resulting from the incisions tend to flatten the optical zone, reducing the refractive power of the eye and thereby reducing the patient's myopia (nearsightedness).

Since its introduction into this country in the late 1970's (Bores, 1983), RK has evolved from an experimental procedure into an acceptable surgical practice among some ophthalmologists. However, its lack of predictability remains a significant problem; see, for example, Arrowsmith and Marks (1985), Deitz et al. (1984), and Sanders and Deitz (1985). Currently, surgeons choose the number and geometry of the incisions from a combination of personal experience and design charts or guides that are based on the statistical results of clinical trials; e.g., Sanders et al. (1984). Such an approach can leave the patient with significant overcorrection or undercorrection (Cross and Head, 1985).

Analytical models of the cornea and surrounding tissues (sclera) have helped put the mechanics of the eye on a firmer theoretical foundation. Shell theory was applied by a number of researchers; e.g., Taber (1984). Although this approach
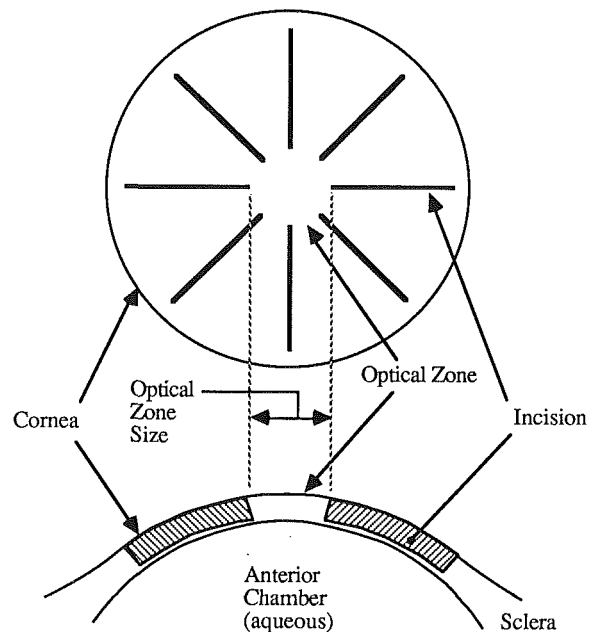

Fig. 1 Typical eight incision RK procedure, illustrating front-on view of cornea (top) and cross sectional view (bottom)

offers some insight into the structural response of the eye, shell theory is not well suited to modeling nonhomogeneity, keratotomy incisions, and other irregular geometric features of the eye. Kobayashi et al. (1971) were apparently the first to apply the finite element method (FEM), which overcomes these difficulties, to the analysis of deformations in the corneoscleral shell. In Kobayashi et al. (1971), an axisymmetric finite element model was used to simulate the structural response of the

---

cornea and sclera to changes in intraocular pressure and to tonometry. Later, the same group employed a similar finite element model to aid in the experimental determination of material property data for the eye (Woo et al., 1972). Both of their models were isotropic and neither included keratotomy incisions.

More recently, researchers have begun to model RK. Schachar et al. (1980) and Huang et al. (1988) model the cornea as an axisymmetric membrane and account for the keratotomy incisions by establishing an effective membrane thickness. In a concept paper, Bryant et. al. (1987) discuss the use of a fully three-dimensional finite element model of the cornea that directly models the incisions. They demonstrate that the deformation pattern resulting from the simulation of RK for a representative eye corresponds to clinically measured corneal topography. Recent work of a similar nature by Vito et al. (1989) confirms this.

In this paper, a number of steps are taken to improve upon previous work in this area. First, a corneal model employing a more general, transversely isotropic constitutive law is implemented via the FEM in a formulation that allows for a more accurate representation of the corneal geometry. Secondly, to more precisely and accurately determine the refractive changes that accompany keratotomy incisions, the corneal model is coupled to an optical model of the entire eye. An optimization-based design approach is then developed to determine the length, depth, and position of the incisions to eliminate a given amount of myopia. It is believed that adopting a design approach to the investigation of RK offers the most direct answer to the fundamental question of RK: how should the operation be performed to correct the patient's vision? To illustrate the procedure, optimal results are presented for a representative eye.

2 The Corneal Model

The human cornea is inherently a complex structure that is composed predominantly of corneal stroma, a composite-like material that consists of approximately 200 randomly oriented lamellae. Each lamella is actually a sheet of collagen fibers that run parallel to one another (Fung, 1981). Additionally, others have observed (e.g., Huang et al., 1988) that when a specimen of corneal tissue is rubbed between two fingers, the two surfaces will slide relative to each other quite easily. This could suggest that there is very little shear stiffness in the stroma and perhaps that the layers of the stroma are sliding relative to each other.

One important issue in modeling soft biological tissues is nonlinear constitutive behavior. Soft biological tissues are known to behave nonlinearly over their entire load range (e.g., Fung, 1981), and corneal tissue in particular has been shown to exhibit a stiffening effect in uniaxial stress-strain tests (Nyquist 1968; Yamada and Evans, 1970) as well as in tests on intact corneas (Jue and Maurice, 1986; Woo et al., 1972). However, our simulations of RK demonstrate that the deformations due to keratotomy incisions are quite small and that the corresponding stresses in the incised cornea do not differ greatly from those of the unincised eye. By comparing these stress levels to the experimentally derived stress-strain curves of Nyquist (1968), Woo et al. (1972), and Yamada and Evans (1970), it was concluded that a linear constitutive law is sufficient for simulating the effects of keratotomy incisions.[2]

It is possible to surmise an appropriate form for the constitutive law by considering the in-plane behavior of the corneal

stroma. The large number and random orientation of the collagen sheets which constitute the stroma suggest that on a macroscopic scale there will be a plane of isotropy oriented with the midplane of the corneal shell. Experimental work by Nyquist (1968) and Woo et al. (1972) supports this. Since the most general continuum-based constitutive law for linear elasticity that is consistent with these observations in transverse isotropy (Chung, 1988), the corneal model described below is linearly elastic and transversely isotropic.

2.1 Transverse Isotropy. From the generalized form of Hooke's law for small strain linear elasticity, the material property tensor can be expressed as a six-by-six, symmetric material property matrix. For transverse isotropy this matrix contains five independent constants and, as shown by Chung (1988), can be written as

$$
\mathbf{E} = \begin{pmatrix}
E_{11} & E_{12} & E_{13} & 0 & 0 & 0 \\
 & E_{11} & E_{13} & 0 & 0 & 0 \\
 & & E_{33} & 0 & 0 & 0 \\
 & & & (E_{11}-E_{12})/2 & 0 & 0 \\
 & \text{symmetric} & & & E_{55} & 0 \\
 & & & & & E_{55}
\end{pmatrix}
$$
(1)

where the xy plane is the plane of isotropy (i.e., there is material symmetry about the z axis), and the five constants are defined as follows:

$$E_{11} = \frac{E_x(1 - \nu_{xz}\nu_{zx})}{C}$$

$$E_{12} = \frac{E_x(\nu_{xy} + \nu_{zx}\nu_{xz})}{C}$$

$$E_{13} = \frac{E_x\nu_{zx}(1 + \nu_{xy})}{C}$$
(2)

$$E_{33} = \frac{E_x\nu_{zx}(1 - \nu_{xy}^2)}{\nu_{xz}C}$$

$$E_{55} = G_{yz}$$

in which E_x is Young's modulus in the xy plane, G_{yz} is the shear modulus in the yz and xz planes, $C = 1 - \nu_{xy}^2 - 2\nu_{xz}\nu_{zx} - 2\nu_{xy}\nu_{xz}\nu_{zx}$, and ν_{xy}, ν_{xz}, and ν_{zx} are Poisson's ratios defined such that ν_{ij} relates resultant strain in the j direction to strain applied in the i direction.

2.2 Equations of Equilibrium. The finite element equations of static equilibrium can be expressed as

$$\mathbf{Kd} = \mathbf{F}$$
(3)

where $\mathbf{K}$ is the global stiffness matrix, $\mathbf{d}$ is the global vector of displacements, and $\mathbf{F}$ is the global load vector.

Since a normal, unincised eye is loaded by its intraocular pressure, the deformations due to RK are relative to this loaded state, and these are the only deformations of direct interest. For this reason, the loaded configuration of the eye is taken as the reference state for the FEM analysis. This is necessary as well since the unloaded geometry of the eye (i.e., without intraocular pressure) cannot be determined under normal circumstances, whereas a patient's cornea in its normal, unincised state can be measured quite accurately using recently developed technology, such as the Corneal Modeling System[3]. Consequently, this approach allows for a more accurate representation of the corneal geometry than other formulations (e.g., Bryant et al., 1987 or Huang et al., 1988) in which the measured

---

[2]Of course, this presumes we are not interested in the stresses near the bottoms of the incisions, where there may be localized regions of high stress. It is believed that such regions are very small and have little effect on the overall deformation of the cornea.
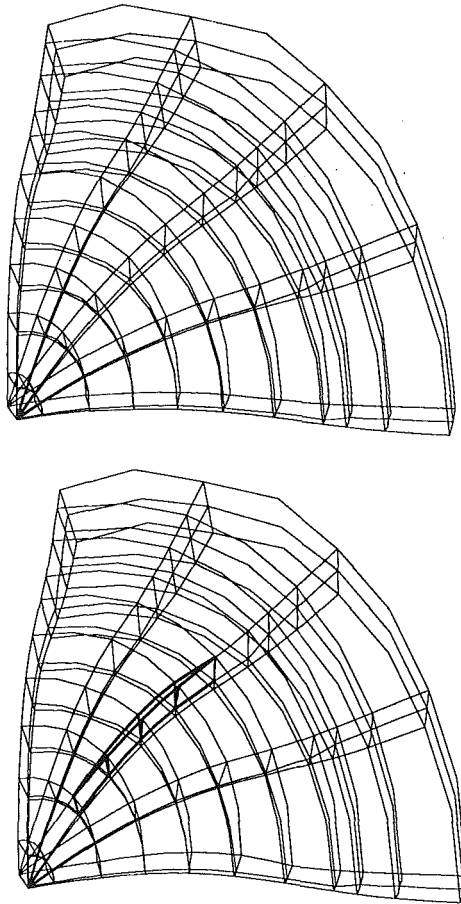
[3]Computed Anatomy Inc.

Fig. 2 Finite element mesh of one quarter of cornea. *Top*: Before introduction of simulated incisions. *Bottom*: Deformed configuration, highlighting one incision of an eight incision procedure (deformations magnified 3×)

These penalty constraints can be expressed as simple element stiffness matrices, so that the global stiffness matrix of equation (3) can be written as

$$\mathbf{K} = \sum_{e=1}^{n} \mathbf{K}_e + \sum_{pn=1}^{npn} \mathbf{K}_{pn}^c \qquad (5)$$

where $\mathbf{K}_e$ is the usual element stiffness matrix that, in this case, defines a 20 node, isoparametric, solid element, $\mathbf{K}_{pn}^c$ is the element defining the penalty constraint between nodes of a constrained node pair, *npn* is the number of penalized node pairs, and the summations represent the FEM assembly process.

The matrices $\mathbf{K}_e$ are written in the usual manner, except that the material property matrix, $\mathbf{E}$, which is given in equation (1) for a coordinate system oriented with the plane of isotropy, must be transformed to the global coordinate system at each integration point in the numerical integration process. Thus, $\mathbf{E}$ is replaced by $\mathbf{T}^T\mathbf{E}\mathbf{T}$, where $\mathbf{T}$ is the transformation matrix (Cook et al., 1989). As implemented, $\mathbf{T}$ is defined by utilizing a *solid geometric model of the cornea to determine the orientation of the plane of isotropy* (Bryant, 1989). This same solid model is used to generate the finite element mesh.

If the degrees of freedom for the penalty constraint "element" are ordered $d_{1x}, d_{1y}, \ldots, d_{2z}$, then the penalty stiffness matrix can be expressed as

$$\mathbf{K}_{pn}^c = \alpha \begin{pmatrix} 1 & 0 & 0 & -1 & 0 & 0 \\ & 1 & 0 & 0 & -1 & 0 \\ & & 1 & 0 & 0 & -1 \\ & & & 1 & 0 & 0 \\ \text{symm.} & & & & 1 & 0 \\ & & & & & 1 \end{pmatrix} \qquad (6)$$

where α is the penalty number, and the two nodes of the "element" are the nodes that define the node pair being penalized. Generally, α is taken to be two or three orders of magnitude higher than other elements of $\mathbf{K}$.

2.3 Material Constants. To approximate incompressible material behavior, a value of 0.49 was chosen for ν_{zx}, which relates strain applied in the z direction to the resulting strain in the x direction. As long as the stresses in the z direction are compressive, this value is probably reasonable. However, it seems unlikely that the stromal material is incompressible with respect to the other two directions of loading. In fact, if the collagen sheets do not interact, then it is likely that the Poisson's effects due to strain applied in the x direction, for example, would be due to only those layers whose fibers are more or less aligned with the x direction. Thus, much smaller values would be expected for ν_{xy} and ν_{xz}. This reasoning led to values for ν_{xy} and ν_{xz} of 1/200 (where 200 comes from assuming only one layer out of 200 contributes to the Poisson's effect) of the incompressible value (0.5), yielding a value of 0.0025 for these constants.

The shear and Young's moduli were chosen so that the FEM model matches Woo's experimental data (Woo et al., 1972). Woo measured the horizontal displacement at a point 2 mm from the apex of intact corneas as a function of intraocular pressure. To utilize these data we chose different values of the shear modulus and, for each one, adjusted Young's modulus so that the horizontal displacement calculated by the FEM solution matched that measured experimentally by Woo at the corresponding pressure. By using these pairs of moduli to simulate RK, a value for the shear modulus of 5 percent of the isotropic value ($E_x/2(1 + \nu_{zx})$) was chosen to provide good qualitative agreement with clinical results. The corresponding Young's modulus is $E_x = 2.01 \times 10^7$ dyn/cm^2.

2.4 Example. Figure 2 illustrates a finite element mesh of

geometry of the cornea is used to represent the *unloaded* configuration of the eye.

In the reference configuration, the intraocular pressure is in equilibrium with the initial state of stress in the cornea that results from the application of the intraocular pressure to the corneal shell. Consequently, the load term in equation (3) contains contributions from both the intraocular pressure and the initial state of stress, and can be written as (Cook et al., 1989)

$$\mathbf{F} = \sum_{e=1}^{n} \left[\int_{S_e} \mathbf{N}^T p \, dS_e - \int_{V_e} \mathbf{B}_e^T \sigma_o^e \, dV_e \right] \qquad (4)$$

where $\mathbf{N}$ is the matrix of shape functions, $\mathbf{B}_e$ is the element strain-displacement matrix, p is the intraocular pressure, σ_o^e is the element initial stress vector, S_e and V_e are the element surface area and volume, respectively, and the summation over the number of elements, n, represents the usual FEM assembly process.

As shown in Fig. 2, incisions are represented in the finite element mesh by allowing elements to separate along interelement boundaries. Extra nodes are added to the global structure at existing node locations on the desired incision surfaces to achieve this. The resulting node pairs define the incision geometry. During the optimization, in which parameters defining the incision geometry are iteratively changed, it may happen that a given incision requires fewer extra nodes to define its geometry than have been added to the mesh initially. In this case, the node pairs that are not needed are constrained to move together via penalty constraints, effectively closing that part of the incision.
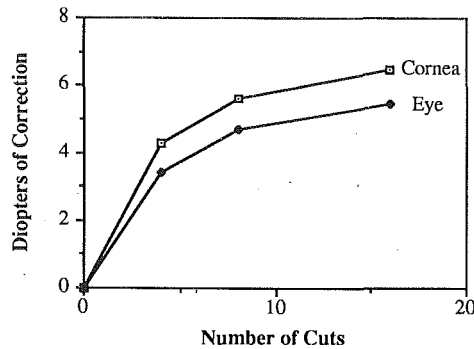
Fig. 3 Effect of number of cuts on dioptic error for example eye $D = 90$ percent of apical value, $P = 0.15$ cm, pressure $= 15$ mmHg, and L is from the optical zone to the limbus.

a quarter of the first author's left eye. Geometric data were obtained from the Corneal Modeling System, which provides a complete topographical map of the cornea. These data were used to create a solid model of the cornea from which the finite element mesh was generated (see Bryant, 1989). The cornea was assumed to possess quarter symmetry, and enough sclera was included in the model to allow fixing the nodes along the sclera's periphery. (Because the sclera is much stiffer than the cornea, if the model includes enough sclera, the degrees of freedom at the boundary of the sclera can be fixed.) Material constants were taken as above, and the intraocular pressure was set at 2.0×10^4 dyn/cm² (15 mmHg). To be consistent with Woo's results, moduli in the sclera were defined to be 3.784 times those in the cornea, and the Poisson's ratios were taken to be the same as those in the cornea. The initial state of stress, as in equation (4), was generated from static equilibrium of the unincised mesh according to equation (3).

As an example of the type of results that can be generated with this approach, Fig. 3 depicts the results of modeling four, eight, and 16 incisions with this model. The vertical axis is a measure of the amount of optical correction achieved, where a diopter is a measure of refractive power, defined as the reciprocal of focal length in meters. To demonstrate the advantages of a complete optical model (described below) in predicting the effects of RK, the data are displayed in terms of both the change in corneal refractive power and the change in refractive power of the whole eye. For eight incisions, the corneal power, given by the upper curve (labeled *cornea*), overpredicts the true optical correction (lower curve) by about 0.9 diopters—a significant amount. The corneal powers were calculated by treating the cornea as a single refracting surface, roughly approximating the clinical measure of corneal power and the technique employed elsewhere in corneal modeling (Bryant et al., 1987; Huang et al., 1988). This discrepancy between corneal refractive power and ocular refractive power has been observed clinically as well (see, for example, Waring et al., 1985) and clearly suggests that corneal geometry alone is insufficient in predicting the optical correction due to RK.

The amount of correction achieved by these simulated RK procedures is well in line with reported results; e.g., Myers (1985). It can also be determined from Fig. 3 that 62 percent of the total correction of a 16 incision procedure is achieved with the first four incisions, while 86 percent is achieved with the first eight. These results compare very closely with those reported by others (see, for example, Deitz et al., 1984). However, it should be noted that healing effects are not considered here, so that these results represent the immediate, and not necessarily long term, effects of RK. A possible way to account for healing in the design process is discussed in the next section. Finally, although the results described here are encouraging, it is recognized that detailed experimental studies are needed to verify the corneal model on a specific case basis. Only then are clinical applications feasible.

3 Design of RK

There is little doubt that before incising a patient's eye the refractive surgeon would like to know how much optical correction the procedure will achieve. An accurate corneal model could solve this problem, although even more critical is the converse problem: how should the procedure be performed to achieve a specific optical correction? The answer to this question entails surgical design. Keratorefractive surgical design can be viewed as an optical design problem coupled to an elasticity problem. For RK, the principal goal is to determine the geometry of the incisions that will deform the center of the cornea (optical zone) into a flatter shape that will in turn eliminate the myopia. In this work, the design of RK is posed as an optimization problem.

Our formulation is based on the following assumptions:
- The cornea has quarter symmetry.
- The incisions have uniform depth.
- The incisions are straight and radial.
- The width of the incisions is infinitesimal.
- All incisions are identical.
- The incisions are uniformly spaced around the optical zone.

These assumptions are consistent with the usual clinical practice of RK which generally consists of either four, eight, or 16 incisions. This parameter is assumed to be given. It should be noted that the assumption of quarter symmetry is primarily for computational efficiency; the following methods could easily be extended to a full corneal model.

A typical incision is shown in Fig. 4, and with the above assumptions, it can be completely described by its length, L, depth, D, and position, P. Thus, the design vector can simply be written as

$$\mathbf{x} = \begin{pmatrix} L \\ D \\ P \end{pmatrix} \tag{7}$$

where L, D, and P are the same for all incisions. Note that since optical zone size is generally given as a diameter, it is $2P$.

Five constraints are imposed on the incisions to prevent them from entering the optical zone, extending beyond the limbus, penetrating the anterior chamber, and to ensure that their lengths and depths have nonnegative values. These constraints can be expressed as follows:

$$\begin{pmatrix} 1 & 0 & 0 \\ 0 & 1 & 0 \\ 0 & 0 & 1 \\ 0 & -1 & 0 \\ -1 & 0 & -1 \end{pmatrix} \mathbf{x} \geq \begin{pmatrix} 0 \\ 0 \\ R_{oz} \\ -D_{max} \\ -R_c \end{pmatrix} \tag{8}$$

where R_{oz} is the radius of the smallest allowable optical zone, R_c is the radius of the cornea, and D_{max} is the maximum incision depth allowed, which is usually defined so that $D_{max} \leq T_c$, the thickness of the cornea at its apex.

The eye's optical system is shown in Fig. 5, in which the cornea and lens provide the refracting surfaces, and the retina is the surface on which the image forms. Since the goal of keratorefractive surgery is to eliminate optical errors in the eye, the objective function for RK is based, in part, on an analysis of an optical model of this system. To facilitate the ray tracing procedure that is developed in Luettgen (1988) for analyzing the optical model, the various refracting surfaces in the eye are modeled by analytic functions (hyperboloids, paraboloids, and ellipsoids). In particular, the refracting surfaces of the cornea are defined by ellipsoids that are fit to the deformed configuration of the finite element model in the optical zone, providing the required coupling between the elasticity problem and the optical model.

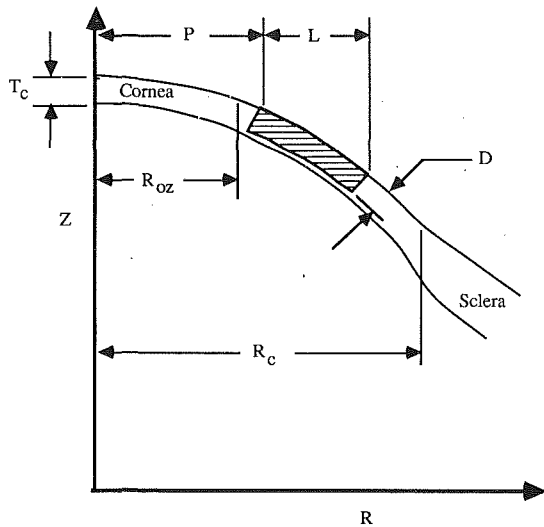In a normal (or emmetropic) eye, rays of light entering the

Fig. 4 Design variables for a typical incision

Fig. 5 The eye's optical system

eye converge to a point on the retina; this is the focal point for the eye, and the plane normal to the optic (z) axis containing this point is the focal plane. On the other hand, the ray tracing in Fig. 5 illustrates myopia, in which the light rays tend to form a focal point in front of the retina. (For comparison, in hyperopia, or farsightedness, the focal point is behind the retina.) Note, however, that, as shown in the figure, this focal point is not necessarily a point, but rather the location along the optic axis where the "diameter" of the bundle of rays is a minimum. (If after the eye is corrected for myopia the focal point is truly a point, then the eye has no astigmatism.)

If the ith ray intersects the $z = z'$ plane at the point $(x_i(z'), y_i(z'))$, as shown in Fig. 5, then the distribution of ray intersection points can be characterized by its "radius of gyration," given by

$$k_0 = \sqrt{\frac{1}{nr}\sum_{i=1}^{nr}(x_i(z')^2 + y_i(z')^2)} \qquad (9)$$

where nr is the number of rays. The focal plane, then, is located at z such that $z' = z_{fp}$, which occurs when $k_0(z)$ is a minimum.

Once the focal plane is found, the myopic error (in diopters) is given by

$$D_{err} = (D_{ret} - D_{corr}) - D_{act} \qquad (10)$$

where

$$D_{ret} = \frac{1}{z_c + |z_{ret}|}, \qquad (11)$$

$$D_{act} = \frac{1}{z_c + |z_{fp}|}, \qquad (12)$$

and where D_{corr} is the amount of overcorrection ($+$) or undercorrection ($-$) desired postoperatively, and z_c, z_{ret}, and z_{fp}, measured in diopters, are as shown in Fig. 5. Note that although the corneal model does not account for healing, D_{corr} could be used to "design in" some overcorrection to compensate for the regressive effects of wound healing.[4]

Since D_{err} is a function of the incision geometry, represented by the design vector $\mathbf{x}$, it may seem that the objective function should contain $D_{err}(\mathbf{x})$ in such a way that when the objective function is minimized, $D_{err}(\mathbf{x}) = 0$. However, an examination of the design space reveals that $D_{err}(\mathbf{x}) = 0$ is satisfied not just for one point x but for some *set* of points $\mathbf{x}$. For example,

long, shallow incisions have the same effect (on D_{err}) as short, deeper ones. Similarly, short incisions placed close to the optical zone have the same effect as longer ones placed farther away. This suggests that $D_{err}(\mathbf{x}) = 0$ represents a manifold in the design space and is thus properly a constraint rather than part of the objective function.

While this accounts for the optical design goals, there are other considerations in the design of keratorefractive surgeries. For example, the ophthalmologist might want to use an optical zone that is as large as possible in order to minimize the possibilities of glare and "starburst," attributed to incisions that directly interfere with the patient's vision (Cross and Head, 1985). Similarly, it might be desirable to minimize the "invasiveness" of the procedure in an attempt to reduce tissue trauma and fluctuation of vision; e.g., Cross and Head (1985). These kinds of design considerations can be termed surgical design goals and are represented here by a scalar function $S(\mathbf{x})$.

Accordingly, the optimization problem for RK can be stated as follows:

$$\min_{\mathbf{x}} S(\mathbf{x})$$

$$\text{subject to:} \quad D_{err}(\mathbf{x}) = 0 \qquad (13)$$

$$Ax \geq b$$

where $Ax \geq b$ is the set of linear geometric constraints, as in (8). Two different cases are now considered for the surgical design functions, $S(\mathbf{x})$.

3.1 Minimizing Invasiveness. The "invasiveness" of a keratorefractive surgery can be defined as the amount of corneal tissue that is cut, and this can be represented by the area of the incision surfaces (i.e., the area of the surfaces that define the incisions). If $S(\mathbf{x})$ is defined to be incision area, then an RK solution that minimizes invasivness can be found by solving the following problem:

$$\min_{\mathbf{x}} L \cdot D \quad (\approx \text{incision area})$$

$$\text{subject to:} \quad D_{err}(\mathbf{x}) = 0 \qquad (14)$$

$$Ax \geq b$$

---

[4]Strictly speaking, of course, one would expect D_{corr} to be a function of $\mathbf{x}$ (as well as other variables not considered here), but the form of this function is beyond the scope of this work.
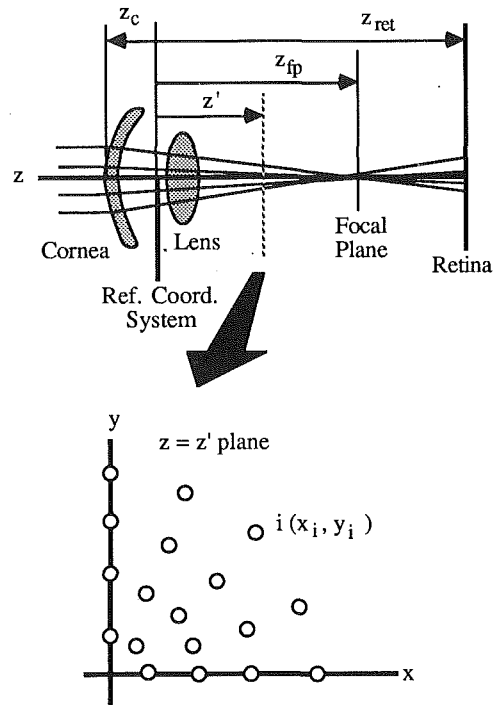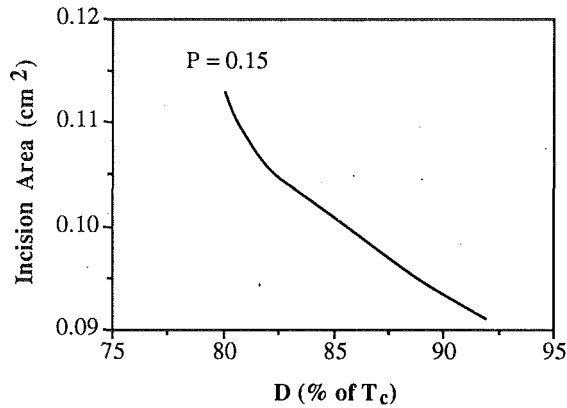
Fig. 6 Monotonicity of incision area over feasible region with respect to depth of cut. Myopia $= -3.4$ diopters; there are eight incisions

where incision area is approximated by $L \cdot D$.

Although equation (14) is a nonlinear optimization problem with both linear and nonlinear constraints, the global minimizer is obtained by utilizing the monotonicity of $L \cdot D$ to identify the active constraints and reduce the dimensionality of the problem to zero (see Papalambros and Wilde, 1979). The resulting constraint bound solution is the global minimizer.

To demonstrate this, the constraint $D_{err}(\mathbf{x}) = 0$ is implicitly substituted into the objective function $S(\mathbf{x})$. Specifically, if $\partial D_{err}(\mathbf{x})/\partial L \neq 0$, then $D_{err}(L,D,P) = 0$ can be written as $L = f(P,D)$, where f is some undetermined function of P and D. Since the incision length clearly affects the optical error, the derivative condition is satisfied. The objective function can therefore be expressed as

$$S(\mathbf{x}) = f(P,D) \cdot D \qquad (15)$$

By implicitly differentiating $D_{err}(\mathbf{x})$ with respect to P the following expression is obtained:

$$\frac{\partial f(P,D)}{\partial P} = -\frac{\partial D_{err}(\mathbf{x})}{\partial P}\left(\frac{\partial D_{err}(\mathbf{x})}{\partial L}\right)^{-1} \qquad (16)$$

which relates the monotonicity of $f(P,D)$ with respect to P to the monotonicities of $D_{err}(\mathbf{x})$.

It can be concluded from typical numerical results (e.g., Fig. 7) that $\partial D_{err}(\mathbf{x})/\partial P < 0$. Similarly, it is clear that $\partial D_{err}(\mathbf{x})/\partial L > 0$ (see Bryant, 1989). Consequently, equation, (16) indicates that

$$\frac{\partial f(P,D)}{\partial P} > 0$$

From (15), then,

$$\frac{\partial S(\mathbf{x})}{\partial P} = \frac{\partial f(P,D)}{\partial P} \cdot D > 0$$

which demonstrates that incision area is monotonically increasing with respect to P.

Thus, to minimize incision area, it is necessary to take the smallest allowable value of P, which from equation (8) is

$$P^* = R_{oz} \qquad (17)$$

Applying the same monotonicity analysis with respect to D leaves the monotonicity (if any exists) of incision area with respect to incision depth indeterminate based on this approach (Bryant, 1989). To resolve this problem, the computationally intensive approach of utilizing the corneal model to calculate incision area versus incision depth is applied (Fig. 6).

It can be seen that incision area is monotonically decreasing with respect to depth, so that the minimum incision area is obtained at the maximum depth of cut. The active constraint that represents this bound is provided by the fourth row of $\mathbf{Ax} \geq \mathbf{b}$, which implies that the optimal incision depth is

$$D^* = D_{max} \qquad (18)$$

Taken together, equation (17) and equation (18) reduce the number of degrees of freedom in the original problem equation (14) by two. Initially, however, there were three variables and one equality constraint and therefore only two degrees of freedom. Consequently, the optimal solution is constraint bound, and the remaining variable, L, can be found by solving the equality constraint, $D_{err}(L,D^*,P^*) = 0$. In summary, then, the solution to equation (14) can be written as

$$D^* = D_{max}$$

$$P^* = R_{oz} \qquad (19)$$

$$L^* = \{L \mid D_{err}(L,D^*,P^*) = 0, \ \mathbf{Ax} \geq \mathbf{b}\}$$

Intuitively, this solution says that minimum incision area is obtained when the incision area is concentrated as close to the center of the eye as possible. Since an incision placed close to the center of the eye is more effective than the same one placed farther away, this might be expected.

Thus, as a consequence of the monotonicity of incision area, the solution to the original nonlinear constrained optimization problem is reduced to the solution of equation (19). From this, L^* can be found by solving the nonlinear equation $D_{err}(L) = 0$ within the limits defined by the linear constraints $\mathbf{Ax} \geq \mathbf{b}$, which specify that

$$0 \leq L^* \leq R_c - R_{oz} \qquad (20)$$

Since $D_{err}(L,D^*,P^*)$ is found to be almost linear, a modified bisection algorithm is used to solve (19) (see Bryant, 1989, for details). Starting with the endpoints given by equation (20), the resulting algorithm generally converges to within 0.125 diopters in no more than five or six iterations. The error tolerance of 0.125 diopters was chosen based on the fact that few people can detect less than 0.25 diopters of myopia. Results for this formulation of RK are presented in the next section, where they are compared to the results of the method developed next.

3.2 Maximizing Optical Zone Size. The most common surgical technique for RK involves cutting the cornea so that the incisions extend from the edge of the optical zone to the limbus (the corneal periphery). Accordingly, the size of the optical zone is an important parameter in this type of surgery, and RK surgeons often design their procedures with an optical zone that is as large as possible. This tends to minimize optical complications, such as glare and starburst, that are caused by incisions that appear in the patient's field of vision (Cross and Head, 1985). For example, the published design guides of Arrowsmith, Deitz, and Sawelson (Sanders et al., 1984) are based largely on this principle. To be more consistent with this clinical approach, an alternative formulation for the design of RK is developed in this section based on maximizing optical zone size.

This is accomplished quite simply by setting $S(\mathbf{x}) = -P$, so that (13) assumes the following form:

$$\min_{\mathbf{x}} -P$$

$$\text{subject to:} \quad D_{err}(\mathbf{x}) = 0 \qquad (21)$$

$$Ax \geq b$$

where the constraint $-L - P \geq -R_c$ of $\mathbf{Ax} \geq \mathbf{b}$ is set active to create incisions that extend to the limbus; thus, $L = R_c - P$. Note that now there is only one degree of freedom in the problem, since there are three design variables and two equality constraints.

As in the previous section, the monotonicity of the objective function can be used to identify an active constraint which indicates that the solution to equation (21) is constraint bound.
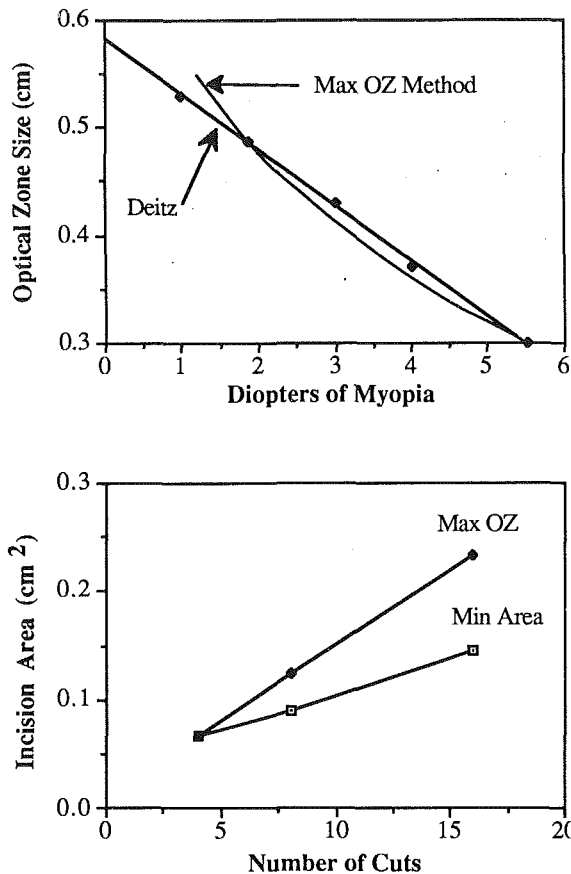
Fig. 7 Optimal results for maximum optical zone method (a) Comparison with Deitz nomogram. (b) Incision area at optimum compared with minimum area formulation

In particular, it can be shown that optical zone size, subject to the constraints $D_{err}(\mathbf{x}) = 0$ and $L = R_c - P$, is monotonically increasing with respect to incision depth, so that the maximum optical zone size is obtained at the maximum depth of cut (Bryant, 1989). Thus, the solution to equation (21) can be written as

$$D^* = D_{max}$$

$$P^* = \{P \mid D_{err}(L,D^*,P^*) = 0, \ L = R_c - P; \ \mathbf{Ax} \geq \mathbf{b}\} \qquad (22)$$

$$L^* = R_c - P^*$$

Here as before, the solution to the original optimization problem is reduced to the solution of nonlinear, algebraic equations: in this case, $D_{err}(L,D^*,P) = 0$ and $L = R_c - P$. In practice, these equations are effectively combined, and a solution algorithm similar to the one described previously is applied towards their solution. Additionally, monotonicity implies that this solution, as in the previous formulation, represents the global minimizer of the original optimization problem (21).

In Fig. 7, optimal results are displayed for the same eye considered previously. For Fig. 7(a), the model simulates an eight incision procedure with an incision depth of 100 percent of the apical value (T_c). It compares the Deitz nomogram (Sanders et al., 1984; Sanders and Deitz, 1985), a widely available design guide for RK that is based on a statistical analysis of clinical data, to the optimal results of the method of this section. Although the two curves are quite close overall, their shapes are somewhat different. Whereas the curve plotted from the Deitz nomogram is nearly linear, the solution to equation (21) indicates that greater increases in optical zone size are required at lower levels of myopia. It should be stated that the Deitz nomogram was chosen for comparison because it is based

on a surgical technique that closely matches the present formulation (21).

As a means of comparing the maximum optical zone formulation to the minimum incision area formulation, incision area at the optimum is plotted in Fig. 7(b) versus the number of incisions for both methods. The data are for an intraocular pressure of 15 mmHg, -3.4 diopters of myopia, and 90 percent depth of cut. At four incisions, the different methods yield the same result only because the maximum incision geometry is required to correct -3.4 diopters of error with four incisions. At eight incisions for this eye, the maximum optical zone formulation requires incisions that are about 30 percent longer than those of the minimum incision area method. Also, it can be seen that the four incision procedure generates the smallest incision area in each case. This seems to suggest that if four incisions will eliminate the myopia, then no more than four should be used. However, this is only strictly true for eyes with perfect axial symmetry, whereas in practice, RK is typically performed on corneas with some astigmatism. In this case, the astigmatism should also be taken into account (see, for example, Bryant and Velinsky, 1989).

4 Conclusions

A general methodology has been presented for the design of the surgical procedure radial keratotomy that relies on coupling a finite element model of the cornea to an optical model of the eye. The following advantages of this approach over previous analytical formulations have been demonstrated:

(1) Adopting a design approach to the investigation of RK allows for the direct determination of the surgical parameters required for optical correction.

(2) The three-dimensional finite element model provides a more accurate representation of corneal geometry, which, among other things, establishes a foundation for extending the approach to astigmatism.

(3) With an optical model of the entire eye, the refractive changes due to keratotomy incisions can be more accurately determined.

The design of RK was formulated as an optimization problem, and two objective functions were considered. In the first formulation, the invasiveness of the procedure was minimized by defining the objective function to be incision area. Optical zone size was maximized in the second formulation. In each case, the monotonicity of the objective function yielded a constraint bound solution, and optimal results were presented for a representative eye.

The results demonstrate that the corneal model is able to replicate clinical trends in RK. Moreover, it is clear that the effects of various parameters on the surgical outcome for a specific eye can be identified, and different RK designs can be compared. Of course, before this can be clinically useful, the corneal model must be experimentally verified. Nonetheless, the results suggest that this approach offers the potential to perform detailed analysis and design of RK on a patient-by-patient basis without the need for statistically derived formulae or nomograms.

5 Acknowledgment

References

1 Arrowsmith, P. N., and Marks, R. G., 1985, "Evaluating the Predictability of Radial Keratotomy," *Ophthalmology*, Vol. 92, pp. 331–338.

2 Bores, L. D., 1983, "Historical Review and Clinical Results of Radial Keratotomy," *Refractive Corneal Surgery: The Correction of Aphakia, Hyperopia, and Myopia*, Binder, P. S., ed., International Ophthalmology Clinics, Vol. 23, pp. 93–118.

3 Bryant, M. R., 1989, *Corneal Modeling and Optimization in the Design of Refractive Keratotomy*, PhD Thesis, Univerisity of Wisconsin-Madison.

4 Bryant, M. R., and Velinsky, S. A., 1989, "Optimal Design of Corneal Refractive Surgery," *Proceedings of the 11th Annual International Conference*, IEEE Engineering in Medicine and Biology Society, Seattle, Nov. 9-12.

5 Bryant, M. R., Velinsky, S. A., et al., 1987, "Computer Aided Surgical Design in Refractive Keratotomy," *CLAO Journal*, Vol. 13, No. 4, pp. 238-242.

6 Burden, R. L., Faires, J. D., et al., 1981, *Numerical Analysis*, Prindle, Weber, and Schmidt, Boston.

7 Chung, T. J., 1988, *Continuum Mechanics*, Prentice Hall, New Jersey.

8 Cook, R. D., Malkus, D. S., et al., 1989, *Concepts and Applications of Finite Element Analysis*, 3rd ed., Wiley, New York.

9 Cross, W. D., and Head, Wm. J., 1985, "Complications of Radial Keratotomy," *Refractive Surgery: A Text of Radial Keratotomy*, Sanders, D. R., ed., SLACK.

10 Deitz, M. R., Sanders, D. R., et al., 1984, "Radial Keratotomy, An Overview of the Kansas City Study," *Ophthalmology*, Vol. 91, pp. 467-478.

11 Fung, Y. C., 1981, *Biomechanics. Mechanical Properties of Living Tissues*, Springer Verlag, New York.

12 Hecht, S. D., and Jamara, R. J., 1982, "Prospective Evaluation of Radial Keratotomy Using the Fyodorov Formula: Preliminary Report," Ann. Ophthalmology, Vol. 14, pp. 319-330.

13 Huang, T., Bisarnsin, T., et al., 1988, "Corneal Curvature Changes Due to Structural Alteration by Radial Keratotomy," ASME *Journal of Biomechanical Engineering.*, Vol. 110, pp. 249-253.

14 Jester, J. V., Venet, T., et al., 1981, "A Statistical Analysis of Radial Keratotomy in Human Cadaver Eyes," *American Journal of Ophthalmology*, Vol. 92, pp. 172-177.

15 Jue, B., and Maurice, D. M., 1986, "The Mechanical Properties of the Rabbit and Human Cornea," *Journal of Biomechanics*, Vol. 19, pp. 847-857.

16 Kobayashi, A. S., Woo, S. L., et al., 1971, "Analysis of the Corneoscleral Shell by the Method of Direct Stiffness," *Journal of Biomechanics*, Vol. 4, pp. 323-330.

17 Luettgen, M. J., 1988, "Computer Aided Modeling and Analysis of the Optics of the Human Eye," M.S. Thesis, University of Wisconsin-Madison.

18 Myers, W., 1985, "Radial Keratotomy: Results and Complications," *Refractive Surgery: A Text of Radial Keratotomy*, Sanders, D. R., ed., SLACK.

19 Nyquist, G. W., 1968, "Rheology of the Cornea: Experimental Techniques and Results," *Exper. Eye Research*, Vol. 7, pp. 183-188.

20 Papalambros, P., and Wilde, D. J., 1979, "Global Non-Iterative Design Optimization Using Monotonicity Analysis," ASME *Journal of Mechanical Design*, Vol. 101, pp. 645-649.

21 Sanders, D., Arrowsmith, P. N., et al., 1984, "Determination of Operative Parameters," *Radial Keratotomy*, Sanders D., ed., SLACK.

22 Sanders, D. R., and Deitz, M. R., 1985, "Factors Affecting Predictability of Radial Keratotomy," *Refractive Surgery: A Text of Radial Keratotomy*, Sanders, D. R., ed., SLACK.

23 Schachar, R. A., Black, T. D., et al., 1980, "A Physicist's View of Radial Keratotomy with Practical Surgical Implications, *Keratorefraction*, Schachar, R. A., Levy, N. S., Schachar, L., eds., LAL Publishing, Denision, Texas, pp. 195-220.

24 Taber, L. A., 1984, "Large Deformation Mechanics of the Enucleated Eyeball," *Journal of Biomedical Engineering*, Vol. 106, pp. 229-234.

25 Vito, R. P., Shin, T. J., and McCarey, B. E., 1989, "A Mechanical Model of the Cornea: The Effects of Physiological and Surgical Factors on Radial Keratotomy Surgery," *Refractive and Corneal Surgery*, Vol. 5, No. 2, pp. 82-88.

26 Waring, G. O., Lynn, M. J., et al., 1985, "Results of the Prospective Evaluation of Radial Keratotomy (PERK) Study One Year After Surgery," *Ophthalmology*, Vol. 92, pp. 177-198.

27 Whitney, J. M., Daniel, I. M., et al., 1982, *Experimental Mechanics of Fiber Reinforced Composite Materials*, Society for Experimental Stress Analysis Monograph No. 4, Prentice-Hall Inc., New Jersey.

28 Woo, S. L., Kobayashi, A. S., et al., 1972, "Nonlinear Material Properties of Intact Cornea and Sclera," *Exper. Eye Research*, Vol. 14, pp. 29-39.

29 Yamada, H., and Evans, F. G., eds., 1970, *Strength of Biological Materials*, Williams and Wilkins, Baltimore, MD.